COMPUTER-AIDED CIVIL AND INFRASTRUCTURE ENGINEERING

Computer-Aided Civil and Infrastructure Engineering **31** (2016) 515–534

A Modified Iterative Closest Point Algorithm for 3D Point Cloud Registration

Roberto Marani*, Vito Renò, Massimiliano Nitti, Tiziana D'Orazio & Ettore Stella

Institute of Intelligent Systems for Automation, Italian National Research Council, Bari, Italy

Abstract: *In this article, an accurate method for the registration of point clouds returned by a 3D rangefinder is presented. The method modifies the well-known iterative closest point (ICP) algorithm by introducing the concept of deletion mask. This term is defined starting from virtual scans of the reconstructed surfaces and using inconsistencies between measurements. In this way, spatial regions of implicit ambiguities, due to edge effects or systematical errors of the rangefinder, are* automatically found*. Several experiments are performed to compare the proposed method with three ICP variants. Results prove the capability of deletion masks to aid the point cloud registration, lowering the errors of the other ICP variants, regardless the presence of artifacts caused by small changes of the sensor view-point and changes of the environment.*

1 INTRODUCTION

The research on the use of laser scanners as a tool to produce 3D point clouds of complex scenes for structural engineering applications has received a great impulse thanks to the continuous improving of laser scanning technology. 3D geometric models from building, terrains, and infrastructure systems, can be used for preventing geological hazards, such as landslides, debris-flows, rockfalls, and floods (Jaboyedoff et al., 2007; Deshpande, 2013). At the same time, the high accuracy of measurements achievable with 3D models permits the reliable check of the conditions of existing buildings and roads (Cai and Rasdorf, 2007; Park et al., 2007; Cord and Chambon, 2012; Nishikawa et al., 2012; Zhang and Elaksher, 2012; Moreno et al., 2013; Truong-Hong et al, 2013; Walsh et al., 2013; Park et al., 2015).

*To whom correspondence should be addressed. E-mail: *marani@ba.issia.cnr.it.*

In the context of infrastructures monitoring, registration of point clouds is a crucial preliminary step to compare data acquired at different epochs and to document changes and geometric deformations of the observed surfaces. The capability of the processing methods to detect variations is strictly dependent on the registration process which has to transform all acquired point clouds to a common coordinates system. In this article, we address the problem, crucial for infrastructures monitoring, of developing a point cloud registration approach which improves the accuracy of 3D data alignments when reliable results are required.

1.1 Related works

Point cloud registration refers to two categories of problems: the precise localization of navigation systems during the acquisition of the dense 3D models of targets and the exact matching of data sets acquired at different epochs for structural monitoring.

The registration of laser scans for the creation of dense 3D models can be increasingly performed by matching the newest scan over the acquired ones while the surroundings are sensed. In this context, the literature on 3D scene recovery is mainly related to trajectory-based methods. Among these methods for laser scan matching, those based on Self Localization And Mapping (SLAM) are the most used (Diosi and Kleeman, 2005; Holz and Behnke, 2010; Rowekamper et al., 2012). They can produce dense 3D models in real time by updating an even more detailed map of the scene together with the information on the sensor position. As an example, a more sophisticated method (Holz and Behnke, 2014) exploits the knowledge on the topology of the scene to simultaneously update both the 3D map and the sensor pose by means of approximate surface reconstructions.

On the other hand, point cloud registration for structural monitoring is aimed to align different data sets,

DOI: 10.1111/mice.12184

even acquired with SLAM methods, to achieve meaningful comparisons on a common reference system. These approaches can be classified as follows (Pfeifer and Böhm, 2008): marker-based, sensor-based, and data-driven registration methods.

Marker-based registrations can be very precise but require that artificial control points, with an easy-to-recognize pattern, are placed in the scene (Kang et al. 2012; Han et al., 2013; Scaioni et al., 2014).

In the sensor-based category (Grinstead et al., 2006; Cazzaniga et al., 2007), the position and orientation of the scanner is determined by GPS and an Integrated Measurement Unit (IMU), limiting the application of these methods to outdoor contexts, where the lines of sight to the GPS satellites are not occluded.

Data-driven approaches use the point clouds properties to find the registration parameters. A widely used algorithm belonging to this category is the ICP (Iterative Closest Point), originally introduced in Chen and Medioni (1991) and Besl and McKay (1992). Given two clouds of points (a reference and a source), the algorithm finds 3D correspondences between the point clouds and tries to determine the translation and rotation matrices whose application to the source can lead to the best match on the reference in terms of minimum distance. Although the method is simple and easy to implement, a drawback resides in the need of a user control for the validation of results, because it often reaches a wrong convergence. Specifically, an erroneous point correspondence between the source and the reference can increase the value of the distance function under optimization, even if the models are overlapping.

Many techniques have been presented to overcome this problem, such as: using the calibration equation of the sensor (Blais and Levine, 1995); weighting the input surface depth data for the integration of the views in a continuous surface (Dorai et al., 1996); including color information, if available, or more generally intensities, in the comparison of the data sets (Johnson and Sing Bing Kang, 1997; Arka, 2005; Gomez-García-Bermejo and Zalama, 2013); extracting invariant features for the selection of points (Sharp et al., 2002); applying geometrical constraints on the point collinearity and closeness (Liu, 2004); employing a global consistency measure to detect incorrect, but locally consistent matches (Huber and Hebert, 2003); using general-purpose nonlinear optimization, such the Levenberg–Marquardt algorithm (Fitzgibbon, 2003). At the same time many speeded-up variants of this method have been also presented (Rusinkiewicz and Levoy, 2001), including the approximation of the nonlinear optimization problem with a linear least-squares one (Low, 2004) and an efficient evaluation of the meaningful points (Xin and Pu, 2010). All these techniques can be also used in the case of registration of scans which are individually subjected to local deformations (Hähnel et al., 2003).

1.2 Our contributions

In this article, we propose a modified ICP algorithm for the registration of data sets acquired at different epochs for structural monitoring. The proposed approach belongs to the data-driven category, i.e., it uses information within point clouds, without artificial markers or GPS/inertial information. As a matter of fact, computer-aided methods that do not use markers can speed up registrations, because the time spent for structuring the environment is no longer required. Furthermore, in this way alignments of point clouds are always enabled, also when the environments cannot be structured or the GPS information is not available (e.g., indoor scenes).

The underlying idea comes from the observation of some limitations common to many ICP approaches. First of all, most of them neglect the properties of the acquisition and the environment under investigation. In fact, when laser rangefinders are used, the mechanisms of ray projection can induce the presence of different shades when objects are observed from altered points of view. As an example, pillars and columns, typical of civil infrastructures (buildings, road and underground infrastructures, such as covered parking, metro tunnels, etc.) can introduce implicit artifacts in the measurements and hence errors in the registration process. In Figure 1, two 3D models of the same environment acquired from different points of view are shown: the red points represent the differences, due to the change of the view-point, which cannot be matched in the registration process. Furthermore, when point clouds are acquired at different epochs for structural monitoring, the inspected scene can experience changes (object shifts, plane rotations, etc.) with respect to the reference point cloud. If both implicit artifacts and actual changes are neglected, and all the points are considered in the registration process, wrong registration parameters can be obtained.

These critical aspects are the main topic of the proposed paper, which modifies the standard ICP implementation by introducing deletion masks, i.e., binary weighting matrices made of 0's and 1's. This strategy is able to remove the measurement artifacts due to the changes of the sensor point of view, reaching higher robustness against the possible environmental changes between the two different acquisitions. Deletion masks are defined at each iteration as a function of the estimated sensor positions and are applied before the evaluation of the distance between the source and reference point clouds. The aim of this mask is the deletion of pairwise comparisons altered as

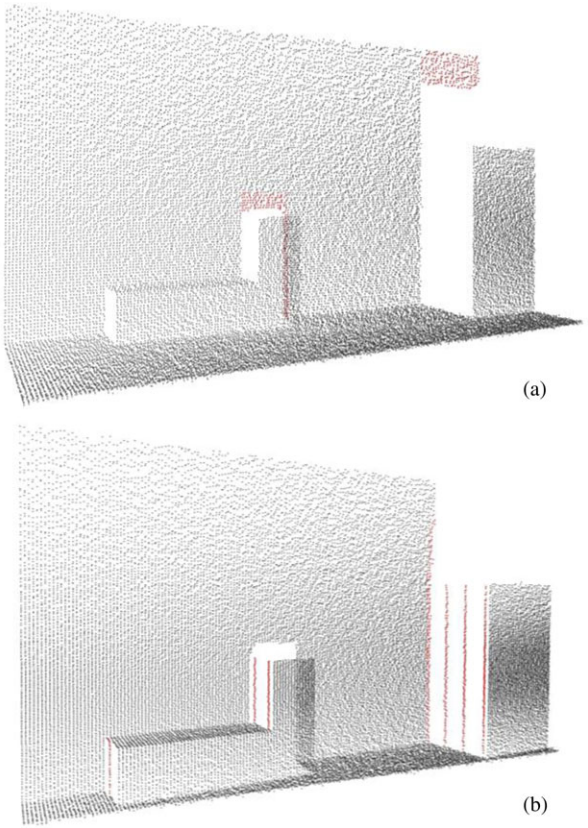

Fig. 1. Comparison of two 3D models of the same environment. Red dots are implicit differences due to the change of the sensor point of view. (a) Reference and (b) source point clouds (see color figure in online version).

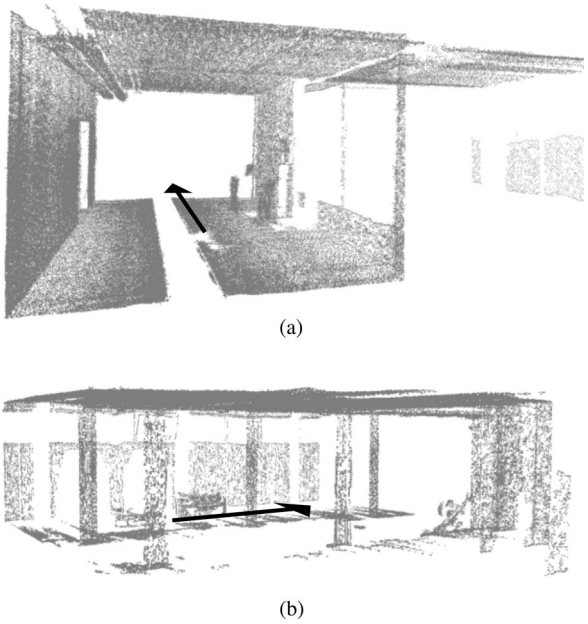

Fig. 2. Example of point clouds derived from (a) a generic indoor environment and (b) a covered parking area The arrows represent the directions followed by the mobile vehicle which carries the sensor through the environment under analysis.

effect of estimated changes of the sensor point of view. Experimental evidence demonstrates that the proposed method can improve the accuracy of the standard ICP method and its variants, also in presence of alterations of the environments under inspection.

The article is organized as follows: Section 2 shows the algorithm in detail, introducing the bases for the formulation of deletion masks; Section 3 describes the experiments and compares the results of the proposed method with those given by the other ICP variants; conclusions and final remarks are shown in Section 4. At the end of the article, the Appendix reports the detailed analytical formulation of virtual measurements.

2 METHODOLOGY

Whenever the processing of 3D models is aimed to monitoring infrastructures, high accuracy and high resolution are necessary. Laser rangefinders are the best sensors to achieve this goal because they can reach and measure hardly-positioned structures in narrow spaces, without any difficulty and regardless of the lighting conditions. Typically, laser rangefinders are bracketed on mobile vehicles, which proceed through the environment, and collect distance measurements ρ as a function of the vehicle position. As a result, the position in space of the samples gives a representation of the acquired targets, namely of their external surfaces. Two examples of point clouds acquired in indoor environments are reported in Figure 2. In particular, Figure 2a represents a generic entrance hall, whereas Figure 2b models a covered parking area. These environments will be the specific case studies for the presented algorithm of point cloud registration. The arrows in Figure 2 display the directions followed by the mobile vehicle during the acquisitions. At this stage, it is important to notice that the method, and its underlying ideas, can be applied to any data set produced by a generic laser scanner. Nevertheless, for the sake of simplicity, the following treatments will refer to the specific case of a moving sensor which collects samples as the vehicle moves through the environment.

The following subsections will describe the best processing for the alignment of two or more data sets modelling the same environment, i.e., an indoor infrastructure. The presented method can find application for any kind of measurement scheme aiming at the environmental modeling. Attention will be focused on the

reduction of the size of the point clouds, together with the description of the main limits of the existing algorithms. Then, the method will be explained in detail, pointing out the most important features that will carry to the improvement of the results.

2.1 Preprocessing steps

The first step in the processing of point clouds aims to simplify the data sets, which is often mandatory to derive lighter data sets, full of information that can be easily treated by the algorithms. Well-known techniques and methods are often used to extrapolate the meaningful parts of the data sets and to simplify them without any loss of information (Moenning and Dodgson, 2004; Song and Feng, 2009; Whelan et al., 2015). This phase can be summarized in the following steps: outlier removal, reduction of useless samples and surface analysis.

Typically, secondary reflections or high-absorbing targets can lead to noisy measurements. As a consequence, many points acquired by the range sensor are outliers which can be removed exploiting the data set statistics (Rusu et al., 2008). As the point clouds are dense of samples, a point is an outlier when it belongs to a low-density region. In practice, a sphere is centered on the investigated point to compare the number of samples within this region with the expected one. In a more efficient way, the acquired samples are clustered following a distance criterion and then processed to find isolated points, i.e., those points, or sets of points, which have a small number of neighbors, lower than a threshold S_{th}. This processing is general and can be applied regardless the kind of scene under analysis. Its effectivity only depends on the properties of the point cloud produced by the sensor: size, resolution and accuracy, which implicitly define the threshold parameters. For instance, laser rangefinders able to produce tens of samples of a surface of 1 cm^2 at 1 m of distance, can return dense point clouds. In this case, setting the radius of the sphere to 1 cm and the threshold $S_{\text{th}} = 5$ can ensure the removal of the only outliers due to measurement errors.

As the method is defined for processing indoor data sets, it is possible to design smart filters, able to exploit this domain knowledge for the removal of those samples that do not add significant information to the model. This result can be achieved by extending the principles of the Split and Merge algorithm (also known as Ramer–Douglas–Peucker algorithm, RDP [Ramer, 1972]) to the input data set. In more detail, the range values belonging to an ordered vector of indices generate a curve which is decomposed in a set of line segments, whose edges define a subset of the exact samples. The simplified curve is derived by deleting the points that have a distance from the corresponding line segment lower than a tolerance value, named as RDP_{tol}. Some results, obtained by changing the tolerance value, are shown in Figure 3. The method operates searching for the most informative points and deleting the ones which are unnecessary. In this way, range sets extracted from indoor transport infrastructures, which are of interest in this framework, are approximated by line segments with low residuals. This representation is the most suitable for the processing of the specific environments, because scenes are usually made of planes. Finally, it is important to observe that the tolerance RDP_{tol} can be chosen proportional to the range measurement, because many sensors produce results with different resolutions, depending on the distance of the target.

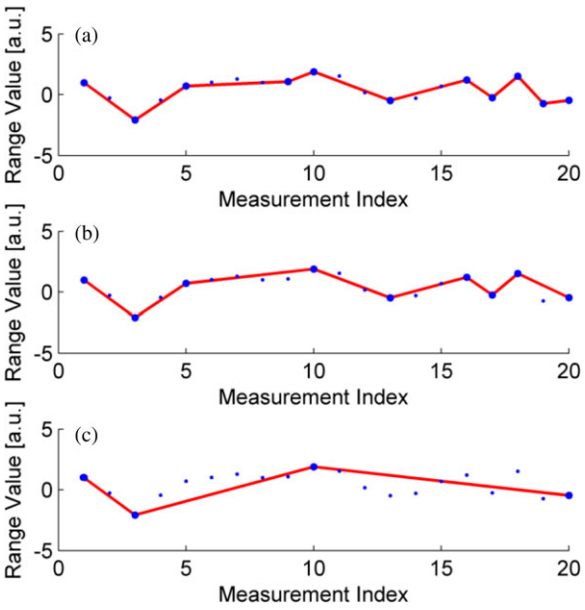

Fig. 3. RDP results on a pseudo-random array of range values. The tolerance value is constant and equal to: (a) $RDP_{tol} = 0.5$, (b) $RDP_{tol} = 1$, and (c) $RDP_{tol} = 2$.

As a final step in the model creation, information about the point position in space are merged with surface data (Horn, 1979). The task of surface reconstruction from 3D range data has been deeply developed and many algorithms have been already proposed. Among them, the most important are the Ball Pivoting Algorithm (Bernardini et al., 1999), the Powercrust (Amenta et al., 2001), the Poisson Surface Reconstruction (Kazhdan et al., 2006; Kazhdan and Hoppe, 2013), and the Multi-level Partition of Unity Implicits (MPU) (Ohtake et al., 2003). When the point cloud is ordered, this goal can be achieved easily. Whenever each range value ρ that belongs to the ith point cloud $\mathbf{P}_i$ (i identifies the acquisition) is obtained at specific discrete indices, a

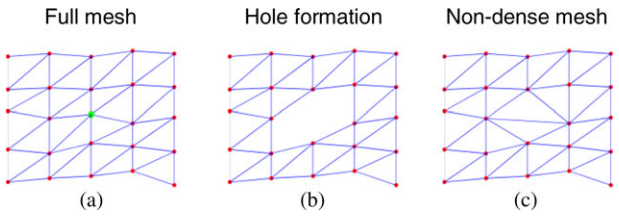

Fig. 4. Example of the process of hole generation due to the simplification of the point cloud (see color figure in online version). (a) Starting mesh; (b) hole formation due to the simplification of the green dot in (a); (c) final result of the surface reconstruction.

surface mesh $\mathbf{S}_i$, made of triangular patches, is directly created by linking consecutive indices (points become vertices of the triangles of the mesh). It is clear that the preliminary simplification produces holes in the map of range values given by the sensor. In this context, Figure 4 reports an example of the generation of holes in the triangular mesh. When the green dot in Figure 4a is deleted by the previous simplification, the reconstruction of the triangular patches fails because the theoretical correspondence of adjacent indices is no longer valid. These issues are overcome by connecting vertices whose indices satisfy a criterion of minimum distance, instead of connecting vertices which are close in space, thus reaching the final result in Figure 4c. In this way, the construction of wrong patches made of edges that actually belong to different surfaces is avoided.

Once the set of ordered connections defined by the surface mesh is defined, it is used to create point normal vectors, which are defined as the average value among all the normal vectors of the triangular patches that include the specific point. Each sample is further compared with the closest ones in terms of normals and it is deleted from the data set if all surroundings have the same properties.

2.2 ICP and its drawbacks

The task of registration of clouds of points is mostly performed applying the ICP algorithm (Chen and Medioni, 1991; Besl and McKay, 1992). A simplified scheme of the standard ICP algorithm is summarized in the flowchart in Figure 5.

Starting from its first formulation, the method considers two point clouds, a reference $\mathbf{P}_0$ and a source $\mathbf{P}_1$, each one constituted by a set (vector) of distance measurements $\boldsymbol{\rho}_0$ and $\boldsymbol{\rho}_1$, respectively. The ICP tries to establish the transformation parameters which carry to the best matching of the overlapping regions, solving an optimization problem in the least squares sense. In summary, the point clouds are first subsampled uniformly or

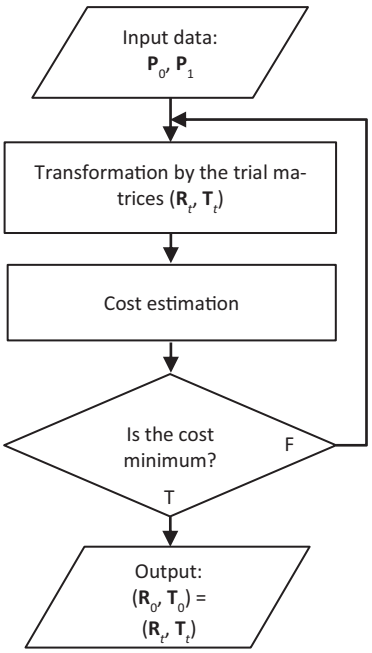

Fig. 5. Flowchart of the standard ICP implementation.

trying to extrapolate the most significant points (discontinuities). Then, the ICP algorithm establishes Γ point correspondences between the two data sets and transforms the source point cloud, following the rotation $\mathbf{R}$ and translation $\mathbf{T}$ guess matrices. Then it directly computes the cost in terms of sum of squared differences between the Γ range values of the matched samples. The cost function is defined as follows:

$$C(\mathbf{R}, \mathbf{T}) = \sum_{j=1}^{\Gamma} (\rho_{0,j} - \rho_{1,j}(\mathbf{R}, \mathbf{T}))^2 \qquad (1)$$

where $\rho_{1,j}(\mathbf{R},\mathbf{T})$ are the range values extracted from the source $\mathbf{P}_1$, after the transformation defined by the guess matrices $(\mathbf{R},\mathbf{T})$. The cost is thus optimized as a function of the trial matrices, which are full of entries. As a consequence, the alteration of the point of view can be compensated exploiting six degrees of freedom.

Further ICP variants exploit a different estimation of the cost function. As an example, a point-to-plane metrics can be used (Low, 2004) to weight the correspondences between homologous points by means of the surface properties. In this case each addend of the cost function is multiplied by a weighting term w_j, equal to the normal vector of the specific jth point of the reference. Here the problem of estimating point normals deserves attention because its accuracy and reliability are mandatory to achieve good results (Mitra et al., 2004).

Although the ICP formulation is very simple and often allows a closed form solution, many drawbacks can emerge in actual contexts (Pomerleau et al., 2013). First

of all, it is straightforward to understand that this cost term is also linked to the possible modifications of the environment. If the environment is heavily altered or the points of view significantly change, the perfect alignment of the data sets produces higher values of the cost function. As an effect, the ICP algorithm can fail because it reaches a minimum of C for incorrect entries of the matrices ($\mathbf{R}$,$\mathbf{T}$).

Moreover, the different points of view of the sensor among the acquisitions can further weight this aspect, because they generate measurement artifacts near the object edges, even if the environment is not altered. This issue is of great importance, because the ICP algorithm filters out these wrong correspondences before the cost estimation by means of median filters. However, when the data sets are obtained from altered environments, the distances among points are higher in values. As a consequence, the median value raises till the limit of being comparable with the distance between points in wrong correspondence. Under these conditions, the use of a threshold to remove from the ICP computation the distances between homologous points higher than the median value does not achieve the expected results. In this case, the effective contribution of this approach vanishes.

Moreover, if the data set is firstly subsampled nonuniformly to preserve information, i.e., discontinuities (Gelfand et al., 2003), the comparison can be additionally affected by errors, because edge regions are the ones carrying the main contributions of implicit ambiguities. Rejecting edges from the comparison, without any smart control, removes almost all the information, inducing registration uncertainty. For this reason the strategy must be improved by taking into account the three dimensions to understand how view-points differ in space, and remove the spatial regions that lead to errors.

2.3 Point cloud registration with deletion mask

As described before, the proposed method intends to overcome the drawbacks of the standard ICP technique and its variants. The method modifies the standard implementation of the ICP algorithm following the processing steps depicted in the flow diagram in Figure 6. Specifically, deletion masks, or DMs (see the dashed box in Figure 6), are introduced to remove the erroneous point correspondences which are extracted from ambiguous regions, where implicit differences can raise as a consequence of the change of the sensor view-point.

Referring to the nomenclature of the previous section, the two data sets $\mathbf{P}_0$ (reference) and $\mathbf{P}_1$ (source) differ by the goal rotation $\mathbf{R}$ and translation $\mathbf{T}$ matrices.

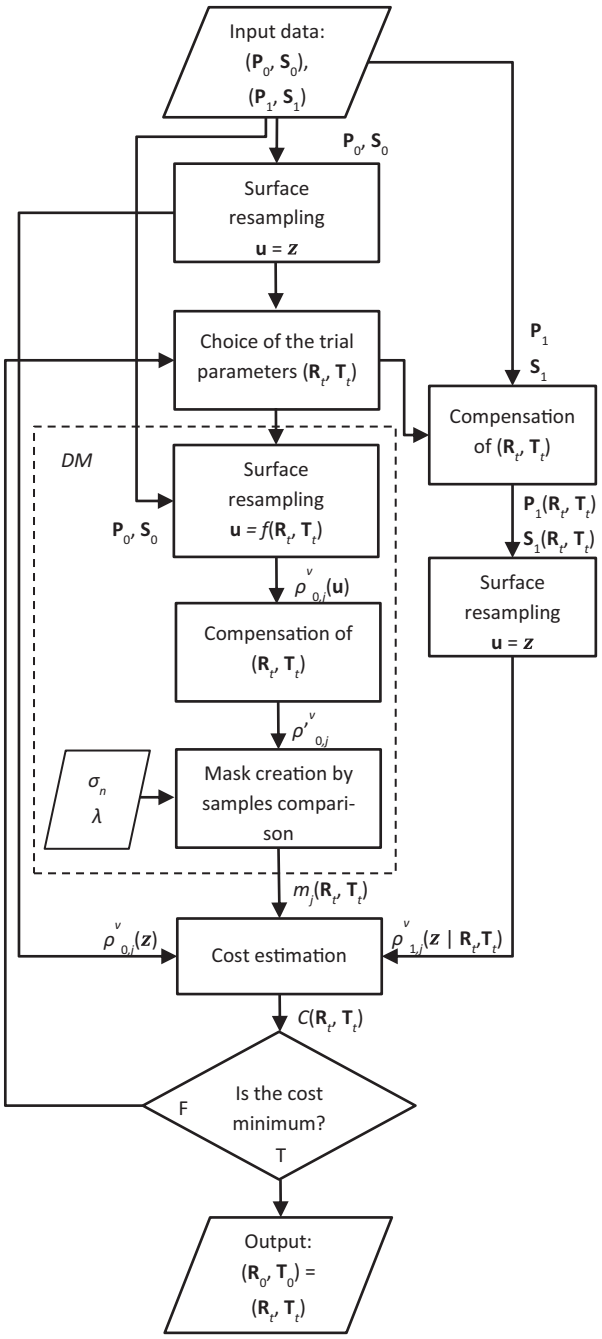

Fig. 6. Flowchart of the presented method for point cloud registration.

Moreover, the starting data set is completed by the corresponding surface meshes $\mathbf{S}_0$ and $\mathbf{S}_1$.

Each box of the flowchart describes a specific operation on the input data, made of the full model (vertices and faces). In summary, the reference and the source point clouds are compared by means of a cost estimation, after that the reference point cloud is analyzed to

derive the deletion mask. As the problem is solved iteratively, trying to find the values of the objective matrices **R** and **T** that approximate the alteration of the sensor point of view, it is possible to exploit **R** and **T** to find the implicit differences due to the change of the sensor trajectory. $\mathbf{S}_0$ is scanned in synthetics, exploiting the concepts of virtual measurement to replicate the expected point of view of $\mathbf{P}_1$, iteratively defined by **R** and **T**. This virtual point cloud is then compensated by the same parameters **R** and **T** and compared to the actual reference. This comparison generates the deletion mask for the specific parameters of **R** and **T**. The mask is thus applied in product in the cost estimation, removing wrong correspondences due to implicit and unavoidable alterations of the point clouds under registration.

It is important to notice that the use of deletion masks in the selection of suitable point correspondences prevents the task from being solved in a closed form. As for the vast majority of the ICP variants, the hypotheses that lead to a close analytical solution are no longer valid, and thus its solution has to be found by means of a trial-and-error approach.

The following subsections highlight the bases of the proposed algorithm, focusing on the two main concepts of virtual measurement and deletion mask.

2.3.1 Virtual measurements. Before going through the description of the methodology, it is mandatory to focus on a preliminary task. Actually, the implementation of the deletion masks follows the definition of *virtual measurements*. The aim of this task is the extraction of a new arrangement of Q samples of the starting surface mesh $\mathbf{S}_i$ from a user-defined point of view.

As the environment is scanned with the aim of a complete reconstruction, it is possible to suppose that the whole surroundings are modeled by a set of surfaces wrapped around a specific direction (e.g., the arrows in Figure 2). Under this hypothesis, the processing intends to create a novel set of points by looking at the whole surfaces from specific positions.

In summary, the virtual scan resamples the reconstructed surfaces starting from positions defined by the direction of a unit vector $\mathbf{u} = [u_x, u_y, u_z]^T$, having origin in a specific initial point p_0. The direction τ of this vector is sampled in $(S + 1)$ points, labelled as p_s, from the origin of $\mathbf{u}$ (p_0) till the end of the spatial domain (p_S). Consequently, $(S + 1)$ planes π_s, orthogonal to τ in the 3D positions of p_s, can be defined. The intersection between these planes and the surface mesh $\mathbf{S}_i$ returns a closed curve, which can be further sampled at discrete angular steps around the direction of $\mathbf{u}$.

As a result, the process gives a new set of range measurements $\rho^v_{i,j}(\mathbf{u})$, where $j = 1, \ldots, Q$. Here the apex v underlines the virtual nature of this measurement.

It is important to notice that this process is intended to replace the original measured points with equivalent ones coming from the intersection with the three-dimensional mesh. Then the registration of data sets will be performed over this new set of points. This process adds an advantage to the methodology in terms of a better response against noise. Specifically, if noise mainly follows a zero-mean Gaussian statistics, each patch takes into account the influence of three points experiencing different corruptions. Consequently, the virtual resampling of the triangular patches acts as a smoothing filter because the noise over the three ranges is "averaged" by the patches. Further numerical analyses have proven a reduction of the dispersion of the set of samples of about 30%.

For further explanation on the process of virtual resampling, the reader can refer to the Appendix.

2.3.2 Deletion masks. Virtual measurements constitute the basis for deletion masks, which are the focus of interest of the presented method. With reference to the diagram in Figure 6, the starting mesh $\mathbf{S}_0$, made of a set of contiguous triangular surfaces, is first resampled at the beginning of the algorithm along a reference path which identifies the direction over which the source point clouds will be registered. Although any direction can be equivalently set as the reference, for the sake of simplicity, $\mathbf{S}_0$ is resampled along the z-axis (compare with the sketch in Figure 20). The resulting set of range values is labelled as $\rho^v_{0,j}(\hat{\mathbf{z}})$. This task is out of the iterative process and thus is computed once when the algorithm starts and aims to determine Q reference samples which will be used to create the deletion masks.

The iterative process begins with the choice of the trial compensation matrices ($\mathbf{R}_t$, $\mathbf{T}_t$), full of nonvanishing entries. The reference $\mathbf{P}_0$ is scanned virtually from the view-point $\mathbf{u}$, defined accordingly with the trial parameters ($\mathbf{R}_t$, $\mathbf{T}_t$). The resulting data set of range values $\rho^v_{0,j}(\mathbf{u})$ is further rototranslated to compensate for the superimposed changes defined by ($\mathbf{R}_t$, $\mathbf{T}_t$), giving a new set of range samples $\rho'^v_{0,j}$. It is easy to understand that the pairwise comparison of $\rho^v_{0,j}(\hat{\mathbf{z}})$ and $\rho'^v_{0,j}$ highlights the only ambiguous regions which can introduce an overestimation of the cost function. Equivalently, $\rho'^v_{0,j}$ is found numerically by looking at exactly the same scene of $\rho^v_{0,j}(\hat{\mathbf{z}})$, but from a different point of view. This replicates on $\mathbf{P}_0$ the same corrupted conditions that are iteratively estimated to affect the source $\mathbf{P}_1$, responsible for the unavoidable implicit differences between the two acquisitions.

Given the information on the ambiguous regions, a deletion mask can be created to prevent these points

from entering in the computation of the cost function. Analytically, the entries of the deletion mask are:

$$m_j(\mathbf{R}_t, \mathbf{T}_t) = \begin{cases} 0, & |\rho^v_{0,j}(\hat{\mathbf{z}}) - \rho'^v_{0,j}| > \lambda \cdot \sigma_n \\ 1, & |\rho^v_{0,j}(\hat{\mathbf{z}}) - \rho'^v_{0,j}| \leq \lambda \cdot \sigma_n \end{cases} \quad (2)$$

being σ_n the noise standard deviation, whose amplitude will be discussed in the next sections, and λ a positive number identifying the mask strength. The latter term should be chosen properly in accordance with the noise statistics. As an example, if range measurements are mostly degraded by white noise, a value of this product greater than three times the variance ($\lambda = 3$) is enough to ensure that differences between couples $\rho^v_{0,j}(\hat{\mathbf{z}})$ and $\rho'^v_{0,j}$ are only due to implicit alterations, out of the statistics with a confidence equal to 99.7%.

The iteration process is finally completed by the surface resampling of the source input mesh. This data set is first rototranslated applying the trial parameters at each iteration. Then, it is resampled following the procedure of virtual measurements with $\mathbf{u} = \hat{\mathbf{z}}$ (misalignments have been already compensated). It is important to notice that the surface resampling of the source mesh still gives Q range values, named as $\rho^v_{1,j}(\hat{\mathbf{z}}|\mathbf{R}_t, \mathbf{T}_t)$, which are implicitly in pairwise correspondence with those extracted from the reference data set ($\rho^v_{0,j}(\hat{\mathbf{z}})$). As a consequence, the point matching is guaranteed without the application of any *a priori* condition.

Starting from its ICP formulation in Equation (1), the cost function can be finally redefined as:

$$C(\mathbf{R}_t, \mathbf{T}_t) = \sum_{j=1}^{Q} m_j(\mathbf{R}_t, \mathbf{T}_t) \times \left(\rho^v_{0,j}(\hat{\mathbf{z}}) - \rho^v_{1,j}(\hat{\mathbf{z}}|\mathbf{R}_t, \mathbf{T}_t)\right)^2 \quad (3)$$

The method can be thus iterated improving the solutions for the cost optimization, within a termination criterion. The final trial matrices $\mathbf{R}_0$ and $\mathbf{T}_0$ that give the minimization of the cost are those of the refined transformation that best approximates the actual values of $\mathbf{R}$ and $\mathbf{T}$.

3 EXPERIMENTS AND DISCUSSION

3.1 Case study

The proposed technique has been developed for the registration of point clouds acquired in the context of indoor infrastructures, where GPS localization is no longer available. The following subsections describe the experimental setup used for the acquisitions, the choice of the preprocessing parameters and the error metrics that will be used for the comparison of results with further ICP variants.

3.1.1 Experimental setup. In the presented experiments, 3D data sets are referred to a local reference system (x_i,y_i,z_i) of the ith acquisition, where the x_iz_i-plane is assumed parallel to the ground. A mobile vehicle proceeds through the environment following straight trajectories along the z_i-axis, and carries a laser rangefinder which samples the surroundings by slices. The origin of the local reference system is placed on the position assumed by the sensor when it acquires the first slice of points. Each slice has N distance measurements expressed in terms of couples (ρ_k,θ_k), $k = 1, \ldots, N$, belonging to planes parallel to (x_i,y_i). Therefore, the resulting point cloud is implicitly ordered in discrete indices, because each range value ρ_k can be labeled by increasing angles θ_k and slices.

Without any loss of generality, the registration is applied to distance measurements performed using the time-of-flight laser scanner AccuRange AR4000-LIR in Figure 7 (AR4000 Laser Rangefinder, 2014). It is made of a laser source working at a wavelength of 780 nm. The generated beam is deflected by 90° by a rotating mirror (2,600 rpm) and then swept through 360°, to sample the environment by slices with a maximum range distance of 15 m. It is worth noticing that acquisitions are actually obtained following a helix, having axis along z_i. Nevertheless, range values are assumed to lie on sampling slices, which are formed anytime the mirror performs a 360°-revolution. The position of the slice origin on the ground is equal to the average value of the x_iz_i-coordinates returned by the vehicle odometry. The vehicle speed has been set to 0.2 m/s, whereas the sample rate of the rangefinder has been fixed to 1 kHz. By combining these parameters, the number of slices of each acquisition is in the range between 200 and 250, which corresponds to a spatial resolution along the direction of the vehicle movement of about 75 mm. Finally the range resolution is equal to 0.25 mm.

Preliminary analyses on the collected samples had demonstrated the existence of three noise sources (Marani et al., 2013):

1. statistical white noise with standard deviation equal to 2.5 mm at a distance of 1 m;
2. colored noise due to the temperature control with a slow time constant of about 2.1 s;
3. an amount of failed acquisitions (5% of the total number of the acquired samples).

Knowing the statistics of the point cloud, it is possible to determine the parameters of the preprocessing steps described in Section 2.1. With more details, the

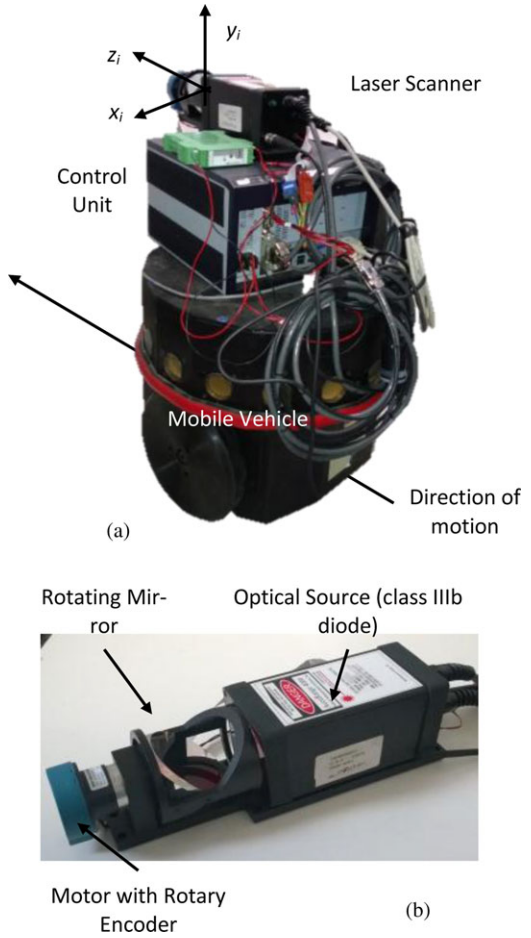

Fig. 7. (a) Experimental setup used for actual inspections. (b) Picture of the laser rangefinder, underlining the optical source and the rotating mirror.

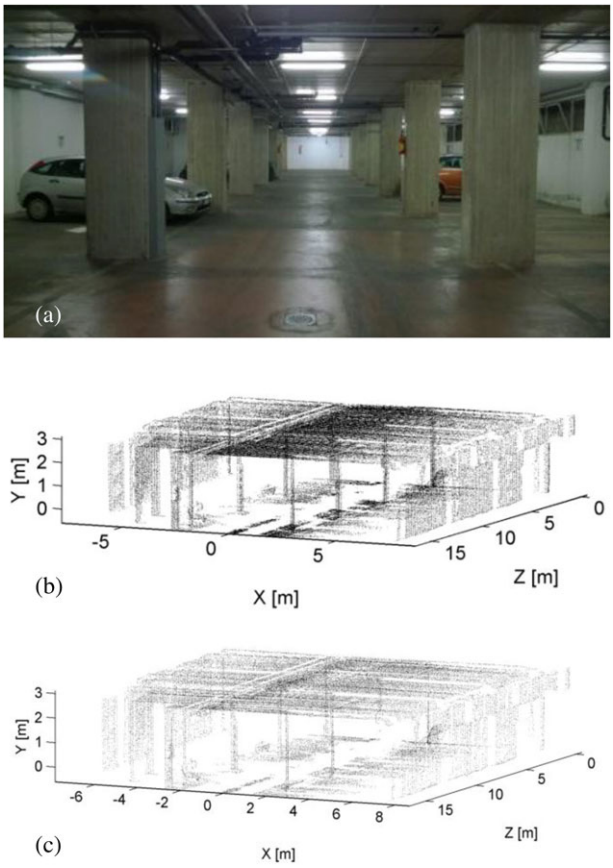

Fig. 8. (a) Covered parking acquired by the laser rangefinder. (b) Corresponding reference data set obtained by the AccuRange AR 4000 laser rangefinder. (c) Simplified point cloud obtained by the application of the preprocessing procedures.

threshold value S_{th} for the choice of the poorer cluster made of outlier candidates is equal to 5. The Ramer–Douglas–Peucker algorithm has been applied to the range values belonging to each slice of the data set with a tolerance value $RDP_{tol} = 1$ mm at 1 m of distance from the sensor source.

It is worth noticing that these parameters are chosen to prevent the lack of information due to the data set simplification. This ensures that the application of the preprocessing steps does not impact the results of the point cloud alignment.

To prove the efficiency of the preprocessing procedures, Figure 8a displays an example of indoor environment acquired with the proposed setup. A covered parking area is modeled by the point cloud in Figure 8b, whose samples are referred to a local system of coordinates, having origin in the center of the first slice of points. The application of the preprocessing steps produces the point cloud in Figure 8c, which is almost three times smaller in size than the starting one. In summary, as an effect of the preprocessing steps, all point clouds considered in these experiments have sizes in the range between 7×10^4 and 10^5 points.

3.1.2 Error metrics for result comparison. The results of the registration processes will be compared with those returned by other ICP algorithms. In this case three variants of the ICP implementation have been considered: the standard linear ICP (Lin-ICP) solved by means of the Single Value Decomposition (SVD) (Chen and Medioni, 1991; Besl and McKay, 1992), the nonlinear ICP (NL-ICP) proposed in (Fitzgibbon, 2003) which is directly solved as a Levenberg–Marquardt (LM) optimization problem, and an optimized linear ICP variant with the point-to-plane (Pt2Pl) metrics (Low, 2004). All algorithms used for the comparison are available online as a part of the point cloud library (PCL) (Rusu and Cousins, 2011).

Fig. 9. Reflective marker used for the point-by-point comparison of registrations.

Following the same strategy adopted by marker-based approaches, several landmarks are used to obtain an effective comparison with a reliable ground truth. In the proposed experiments, the environment under analysis has been structured with seven high-reflection markers (see Figure 9), named as M_k, $k = 1, \ldots, 7$, whose position is chosen to investigate all degrees of freedom (four markers on the side walls of the parking area, two on the ground, and one on the floor) and to obtain their detection from each point of view. These markers can be easily distinguished within the data sets by looking at the intensity of the laser spot (this value is returned by the sensor for each range sample). Hence, the error metrics is defined as the distance (d_x, d_y, and d_z along the three corresponding axes) between homologous markers extracted from the reference cloud $\mathbf{P}_0$ and the source one, after its registration. Specifically, the exact marker position is assumed as the center of mass of the cluster which model the marker. In this way the measurement uncertainty is divided by the number of points of the cluster, thus becoming negligible in the evaluation of the registration error.

Furthermore, it is worth noting that the position of the markers in the point clouds is established through odometry, because the data set creation makes use of the position of the vehicle to translate range values into spatial 3D coordinates. This gives in turns an error in the localization of such points, because the vehicle position is determined with the measurement uncertainty of the encoders. Nevertheless, the comparison of results obtained by the proposed method and the other ICP variants is consistent, because all the methods are applied on the same data sets. As a consequence, the uncertainty will produce the same bias errors in the distance measurements between the homologous markers.

3.1.3 Model optimization. Although the formulation of the presented method is general and can be applied in any context, given the specific case of study, some simplifications are imposed to increase efficiency by reducing the computational requirements.

As a first step, it is possible to take advantage of the measurements purposes. As stated before, environmental monitoring aims to understand whether a change affects the scene under analysis. Consequently, the vehicle has to sense the environment from points of view that have to be close to the one of the reference. In this case the comparison makes sense because the same targets, which are constitutive of the scene, can be compared. As a consequence, all paths followed by the vehicle are almost comparable, but not equal.

Moreover, in the scenario of environmental monitoring, 3D reconstructions will be performed exploiting the same experimental setup, i.e., with fixed elevation of the sensor on the mobile vehicle. Hence, consecutive measurements are affected by relative alterations of the reference system in the xz-plane. Analytically, any alteration of the vehicle trajectory can be compensated by means of two translations X, Z along the x_i- and z_i-axis, respectively, and a rotation H around the y_i-axis. This hypothesis introduces a simplification in the registration scheme and consequently reduces the computational time required to perform the cost optimization described in Section 2.3, without a corresponding degradation of the final results, as it will be shown in the next subsections.

3.2 Experiments and results

Several experiments have been run to compare the results of the registration obtained with the proposed method with those returned by three ICP variants.

Two different conditions are discussed in the next subsections to prove the robustness of the registration. In the first case the data sets are extracted from the same environment (static environment), sensed from different points of view, i.e., trajectories. Then, the acquisitions will be performed still on the same environment, but introducing some alterations (changing environment).

Finally, acquisitions of an indoor environment, the entrance hall of a building under construction, will be registered, to further compare the proposed methodology with the existing ones.

3.2.1 Acquisitions of static environments. In the first experiments, the data set registration is performed on static environments, i.e., perfectly equal scenes. As an effect, although surroundings do not change with respect to the reference data set, relative differences among the point clouds arise because of the alteration of the vehicle trajectories and the measurement noise.

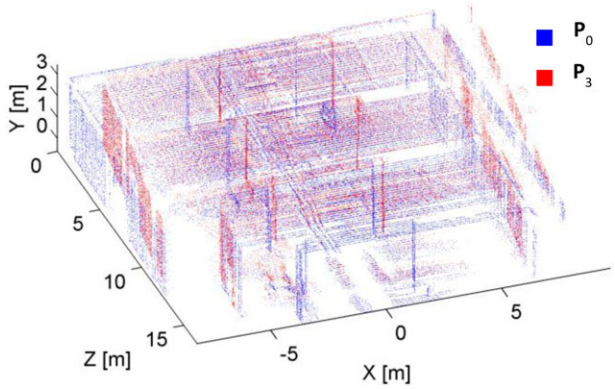

Fig. 10. Original data sets in the local reference systems of the laser rangefinder. Blue and red dots belong to different data sets to be registered, namely $\mathbf{P}_0$ and $\mathbf{P}_3$, respectively (see color figure in online version).

Three source data sets $\mathbf{P}_1$, $\mathbf{P}_2$, and $\mathbf{P}_3$, in addition to the reference $\mathbf{P}_0$, have been acquired at different epochs following different trajectories. Here, to prove the robustness of the method, $\mathbf{P}_3$ has different spatial resolution along the direction of motion of the vehicle. In particular, its size is almost halved with respect to $\mathbf{P}_0$. As an example, the comparison of the data sets $\mathbf{P}_0$ and $\mathbf{P}_3$ is shown in Figure 10.

Following the theoretical description in Section 2.3, the deletion masks have been determined starting from the choice of the trial parameters X_t, Z_t, and H_t. In this case the number of points Q drawn from the input data sets in the surface resampling task has been imposed equal to 38,400, corresponding to 160 slices having 240 samples. An example of deletion mask is reported in Figure 11, where the points of the resampled data extracted from $\mathbf{P}_0$ are colored accordingly with the values assumed by the mask.

Figure 12 shows the first results of the registration of $\mathbf{P}_3$ on the reference $\mathbf{P}_0$ performed by the linear ICP algorithm and the proposed variant, which employs the deletion masks (see Figures 12a and b, respectively). Although the results seem to be comparable, the estimated correction parameters differ in values. This consideration is further proved by the analysis of Table 1, which reports the correction parameters estimated by the four considered ICP algorithms. In particular, the parameters obtained by the Lin-ICP and the DM-ICP produce the vehicle trajectories described by the vectors in Figure 13.

Table 2 summarizes the minimum, maximum, and average values of the distances computed between corresponding reflective markers extracted from the reference data set and the registered ones. Bold values indicate the best results achieved by the comparisons.

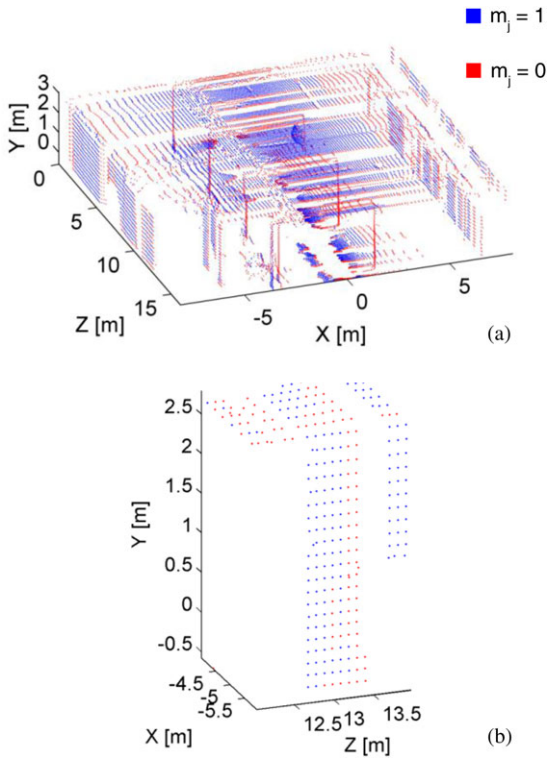

Fig. 11. (a) Effects of the masking process: red points are neglected in the pair-wise registration of data sets; (b) magnified view of the deletion mask applied to the samples extracted from the reference (see color figure in online version).

Table 1
Results of the registrations of the source data sets $\mathbf{P}_1$, $\mathbf{P}_2$, and $\mathbf{P}_3$ on the reference data set $\mathbf{P}_0$. X_0 and Z_0 are expressed in millimeters (*Lin*: standard linear ICP; *NL*: nonlinear ICP; *Pt2Pl*: Point-to-Plane metrics; *DM*: Deletion Mask)

	Lin	*NL*	*Pt2Pl*	*DM*
		X_0		
$\mathbf{P}_1$	–1121.1	–998.06	–1239.06	–1230.1
$\mathbf{P}_2$	61.14	29.25	109.75	138.11
$\mathbf{P}_3$	–1341.7	–1118.27	–1570.83	–1598.3
		Z_0		
$\mathbf{P}_1$	152.81	118.53	191.85	242.61
$\mathbf{P}_2$	259.08	196.4	441.96	461.68
$\mathbf{P}_3$	240.38	174.2	356.87	370.72
		H_0		
$\mathbf{P}_1$	4.94°	4.29°	5.67°	5.49°
$\mathbf{P}_2$	–2.35°	–2.01°	–2.75°	–3.09°
$\mathbf{P}_3$	4.73°	3.5°	6.13°	6.19°

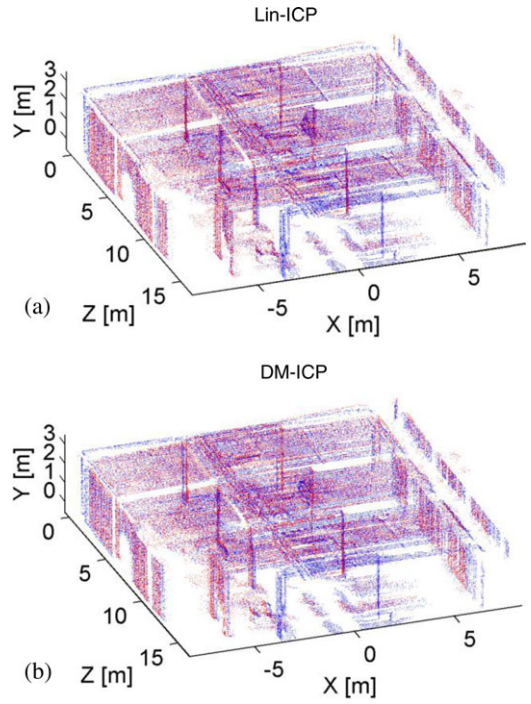

Fig. 12. (a) Results of the data set registration performed with the Lin-ICP algorithm. (b) Point clouds registered by the use of the proposed algorithm based on the use of deletion masks (see color figure in online version).

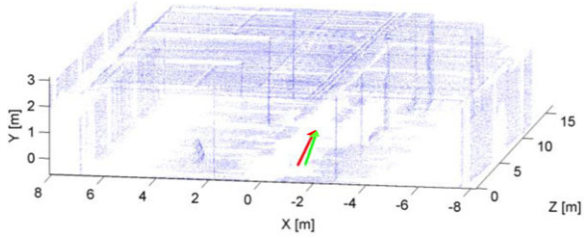

Fig. 13. The red and green arrows are the robot trajectories within the reference point cloud, estimated by the Lin-ICP and the proposed method, respectively (see color figure in online version).

Table 2
Minimum, maximum, and mean distance values [mm] between corresponding reflective markers extracted from the registrations of $\mathbf{P}_1$, $\mathbf{P}_2$, and $\mathbf{P}_3$ on $\mathbf{P}_0$. Best results are highlighted in bold (*Lin*: standard linear ICP; *NL*: nonlinear ICP; *Pt2Pl*: Point-to-Plane metrics; *DM*: Deletion Mask)

		Lin	*NL*	*Pt2Pl*	*DM*
			d_x		
$\mathbf{P}_1$	*Min*	69.85	92.93	4.75	**2.23**
	Max	343.17	251.66	**75.41**	76.33
	Mean	192.77	156.33	39.88	**37.94**
$\mathbf{P}_2$	*Min*	**2.82**	5.89	6.37	19.48
	Max	**63.44**	112.96	77.78	125.19
	Mean	**30.01**	38.7	30.48	44.77
$\mathbf{P}_3$	*Min*	57.73	157.39	17.26	**10.05**
	Max	246.7	426.76	89.62	**63.89**
	Mean	152.39	273.28	45.9	**36.85**
			d_y		
$\mathbf{P}_1$	*Min*	**0.24**	3.32	0.53	1.08
	Max	**8.92**	21.94	21.43	21.59
	Mean	**2.34**	8.55	6.41	6.45
$\mathbf{P}_2$	*Min*	**1.99**	5.98	3.89	3.76
	Max	40.27	33.87	29.05	**28.72**
	Mean	20.43	16.16	17.47	**15.06**
$\mathbf{P}_3$	*Min*	**0.08**	0.85	3.02	1.7
	Max	**23.9**	43.01	50.01	33.05
	Mean	**6.92**	22.54	17.23	13.83
			d_z		
$\mathbf{P}_1$	*Min*	1.62	2.49	13.75	**0.41**
	Max	104.88	205.21	105.53	**58.25**
	Mean	38.47	118.1	60.55	**34.31**
$\mathbf{P}_2$	*Min*	69.7	175.78	1.04	**6.43**
	Max	301.18	348.24	136.18	**130.88**
	Mean	186.78	260.21	41.15	**39.5**
$\mathbf{P}_3$	*Min*	**10.35**	99.12	14.6	10.82
	Max	237.19	321.71	133.61	**112.55**
	Mean	117.02	194.91	68.2	**62.97**

The insight into the results of Table 2 reveals that the use of the deletion masks can improve the estimation of the registration parameters, because the distance components d_x and d_z are always lower when the deletion masks are used. This scenario is altered only in the case of the analysis of $\mathbf{P}_2$, whose registration performed by the linear ICP induces the lowest values of the term d_x. However, the decrease of the mean value of d_x is much lower in magnitude than the improvements produced by the DM-ICP in the remaining cases (see the registrations of $\mathbf{P}_1$ and $\mathbf{P}_3$).

At the same time, results in Table 2 show a different behavior of the distance term computed along the y-axis (d_y). The linear ICP often carries to the best results in comparison with the other methods, although improvements are in any case below those obtained for the comparison of the other two components d_x and d_z. This behavior is mainly ascribable to the experimental setup used for the experiments. In fact, the only contribution responsible for the distance component d_y is the measurement noise. It is clear that changing the algorithm, making it heavier, with the sole intention of compensating for noise would not produce appreciable improve-

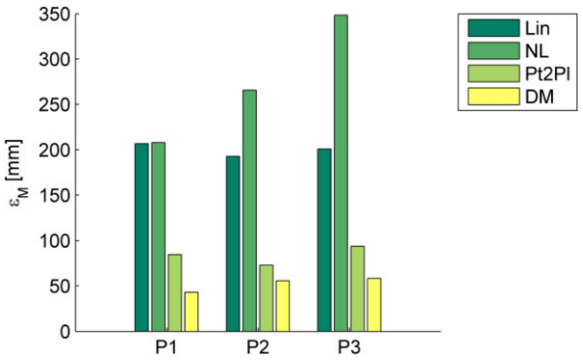

Fig. 14. Comparison of results obtained by the use of the four ICP variants. The bar plot displays the values of the figure of merit ε_M, defined to compare the registration outcomes.

ment of the overall results. In other terms, although the analytical formulation of the Lin-, Nl- and Pt2Pl-ICP considers rototranslation matrices full of nonvanishing entries, it does not improve significantly the results.

An easier comparison can be derived by means of the figure of merit ε_M which depends on the global average value of the distance vectors made of the three components (d_x, d_y, d_z). Analytically, it is equal to:

$$\varepsilon_M = \underset{M_k}{\text{mean}} \left\{ \sqrt{d_x^2 + d_y^2 + d_z^2} \right\} \tag{4}$$

where the mean function is first computed among the corresponding marker distances. This figure of merit is plotted in Figure 14.

The analysis of the results states a clear reduction of the distance errors. Specifically, averaging the ε_M values among the three registrations, the mean values of ε_M are equal to 197.02 mm for the Lin-ICP, 273.94 mm for the NL-ICP, and 83.75 mm for the Pt2Pl-ICP, whereas the homologous term for the proposed algorithm is equal to 62.46 mm. Also this result proves that the initial hypothesis of alteration of the vehicle trajectory in the xz-plane, does not lead to appreciable registration errors.

Finally, it is important to notice that the numerical gap found by the comparison of the ε_M values is much higher than the measurement uncertainty produced by the sensor, close to few millimeters. As a consequence, this result is only attributable to the effective contribution brought by the methods to the registration process.

3.2.2 Acquisitions of changing environments. The comparison of changing environments, i.e., scenes with small differences, is the most challenging problem in the data set registration, because the cost function takes into account also the presence of scene alterations. In this case, the distance between the two considered point

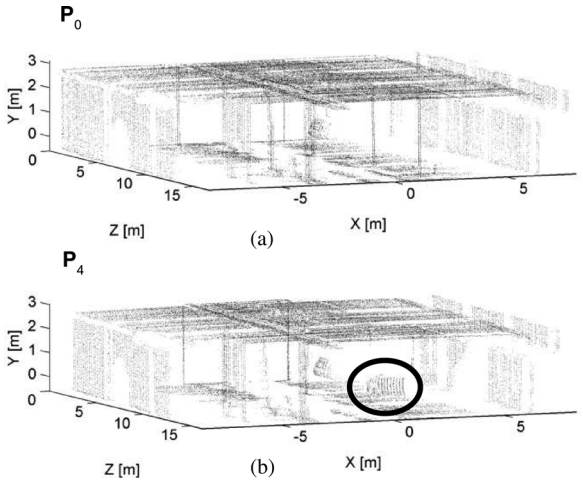

Fig. 15. Comparison between (a) the reference $\mathbf{P}_0$ and (b) the source point cloud $\mathbf{P}_4$. The circle includes the altered points.

clouds can be significantly different from zero, till the limit of turning into a local minimum. In this case, the ICP algorithm reaches the convergence with registration parameters which can be significantly different from the correct one.

These experiments have considered three new acquisitions, namely $\mathbf{P}_4$, $\mathbf{P}_5$, and $\mathbf{P}_6$, acquired at different epochs within the same environment, after that the position of several foreground objects has changed. In particular, another car is added in the parking, producing an alteration of 2% of points of the reference data set. Quantitatively, the point cloud $\mathbf{P}_4$ shows 1,463 altered points over the total size of 79,073 samples. A comparison between the data set $\mathbf{P}_4$ and the reference $\mathbf{P}_0$ is reported in Figure 15, where the two point clouds are displayed.

Also in this case, the $\mathbf{P}_6$ data set has been created by halving the spatial resolution along the straight trajectory followed by the vehicle, i.e., doubling the speed of the vehicle that carries the sensor, but keeping the remaining set of measurement parameters. The results of the registration process are thus reported in Table 3, where the estimated parameters derived by the four methods under analysis are shown.

Results are once more in contrast and produce different distances between corresponding markers. As shown in Table 4, which describes the minimum, maximum, and mean distance contributions computed among the homologous markers of different data sets, the use of deletion masks can reduce the registration errors. This consideration is verified for the analysis of the d_x component, whose values obtained by the DM-ICP are better than the others in most cases. On the contrary, the inspection

Table 3
Results of the registrations of the source data sets $\mathbf{P}_4$, $\mathbf{P}_5$, and $\mathbf{P}_6$ on the reference data set $\mathbf{P}_0$. X_0 and Z_0 are expressed in millimeters (*Lin*: standard linear ICP; *NL*: nonlinear ICP; *Pt2Pl*: Point-to-Plane metrics; *DM*: Deletion Mask)

	Lin	*NL*	*Pt2Pl*	*DM*
		X_0		
$\mathbf{P}_4$	–154.06	–123.95	–173.29	–237.29
$\mathbf{P}_5$	–935.13	–820.66	–1062.38	–1085.5
$\mathbf{P}_6$	118.53	–253.26	107.22	86.2
		Z_0		
$\mathbf{P}_4$	219.71	167.16	515.26	482.02
$\mathbf{P}_5$	142.2	109.1	232.78	291.26
$\mathbf{P}_6$	315.91	207.09	674.43	674.42
		H_0		
$\mathbf{P}_4$	1.5°	1.27°	1.65°	2.3°
$\mathbf{P}_5$	2.3°	1.8°	2.96°	2.95°
$\mathbf{P}_6$	–5.54°	–3.6	–8.05	–7.81°

of results shows again comparable values of d_y obtained by the four methods, although Lin-, NL-, and Pt2Pl-ICP exploit the full transformation matrices, whereas the proposed technique simplifies the problem to the optimization of only three terms. Although measurement noise determines a contribution to the overall cost function, which cannot be compensated by the DM-ICP, its outcomes are in any case comparable. Once again it justifies the initial downgrade of the problem to the compensation of the vehicle trajectory with only three degrees of freedom.

Results obtained by the Pt2Pl-ICP and the DM-ICP in terms of the d_z component are highly comparable in magnitude. In this case, it is important to observe that the point-to-plane metrics allows the reduction of the contributions to the objective cost function of erroneous correspondences between samples. This filtering effect is noticeable especially in these last experiments, when the environments under testing show relative changes. In principle, the method weights such correspondences, exploiting the surface similarity. With more details, the point distance is multiplied by a term (dot product of surface normals) which is 0 when the two surfaces are orthogonal and 1 when the two surfaces are parallel. At a first glance, this metrics seems to limit wrong correspondences in the cost computation in a similar way to the DM approach, thus producing comparable results. Actually, given the weight formulation, the Pt2Pl metrics is not able to discriminate the presence of scene changes due to the movement of objects having parallel surfaces to the ones placed in the corresponding regions of the reference point cloud.

Table 4
Minimum, maximum, and mean distance values [mm] between corresponding reflective markers extracted from the registrations of $\mathbf{P}_4$, $\mathbf{P}_5$, and $\mathbf{P}_6$ on $\mathbf{P}_0$. Best results are highlighted in bold (*Lin*: standard linear ICP; *NL*: nonlinear ICP; *Pt2Pl*: Point-to-Plane metrics; *DM*: Deletion Mask)

		Lin	*NL*	*Pt2Pl*	*DM*
			d_x		
$\mathbf{P}_4$	*Min*	18.02	38.55	4.9	**1.19**
	Max	55.66	83.35	72.35	**72.08**
	Mean	36.46	51.36	35.67	**33.96**
$\mathbf{P}_5$	*Min*	9.62	17.29	**6.89**	7.91
	Max	205.36	294.92	109.33	**83.49**
	Mean	95.14	141.38	41.32	**38.21**
$\mathbf{P}_6$	*Min*	45.8	71.47	**5.06**	14.12
	Max	126.27	149.42	49.6	**49.23**
	Mean	78.55	110.44	28.23	**25.93**
			d_y		
$\mathbf{P}_4$	*Min*	2.90	4.06	1.26	**1.25**
	Max	**24.29**	28.57	26.58	33.32
	Mean	13.95	14.48	**10**	14.24
$\mathbf{P}_5$	*Min*	0.46	**0.34**	2.67	2.81
	Max	**38.03**	59.04	63.96	62.47
	Mean	**18.16**	20.13	24.07	22.13
$\mathbf{P}_6$	*Min*	**0.7**	24.75	3.23	13.81
	Max	**14.38**	27.31	14.96	16.4
	Mean	**5.59**	26.03	8.14	15.72
			d_z		
$\mathbf{P}_4$	*Min*	73.88	141.06	**1.46**	9.73
	Max	302.65	364	166.24	**160.59**
	Mean	200.59	275.02	59.76	**59.02**
$\mathbf{P}_5$	*Min*	34.09	36.48	**11.26**	59.33
	Max	126.49	457.62	190.22	**132.22**
	Mean	91.96	148.09	**38.3**	71.48
$\mathbf{P}_6$	*Min*	132.43	149.82	**68.56**	90.3
	Max	422.07	524.92	270	**233.8**
	Mean	310.31	337.37	**136.53**	174.24

Consequently, the point-to-plane metrics fails and the cost term can grow as much as the objects position changes. On the contrary, the use of virtual resampling and DMs can automatically and *perceptively* remove wrong point correspondences, regardless the relative direction of the surface normals. Nevertheless, results in Table 4 demonstrate that the point-to-plane error metrics can add reliability to the convergence of ICP algorithms. Its implementation in the proposed method will be the aim of future investigations.

Then, with reference to the outcomes displayed in Figure 16, where the figure of merit ε_M is presented, the use of deletion masks improves the registration process in two cases out of three. Quantitatively, the average

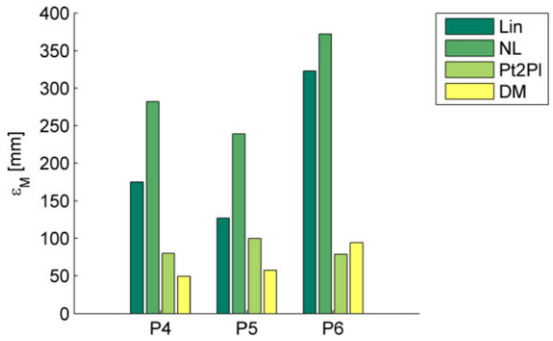

Fig. 16. Comparison of results obtained by the use of the four ICP variants. The bar plot displays the values of the figure of merit ε_M, defined to compare the registration outcomes.

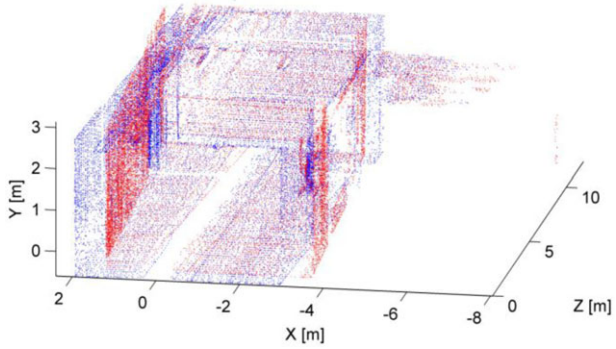

Fig. 17. Original data sets acquired from an entrance hall. Point clouds are referred on the local reference system of the sensor (see color figure in online version).

value among registrations of ε_M reaches 223.28 mm in the case of the Lin-ICP, 297.6 mm for the NL-ICP, 86.27 mm for the Pt2Pl-ICP, and 65.06 mm for the proposed algorithm. By a comparison of these results with those displayed in the previous subsection, it can be stated that the proposed method is robust against consistent scene alterations, because the average value of ε_M does not change as scene differences arise.

3.2.3 Further analysis of an indoor environment. The proposed method has been further tested for the

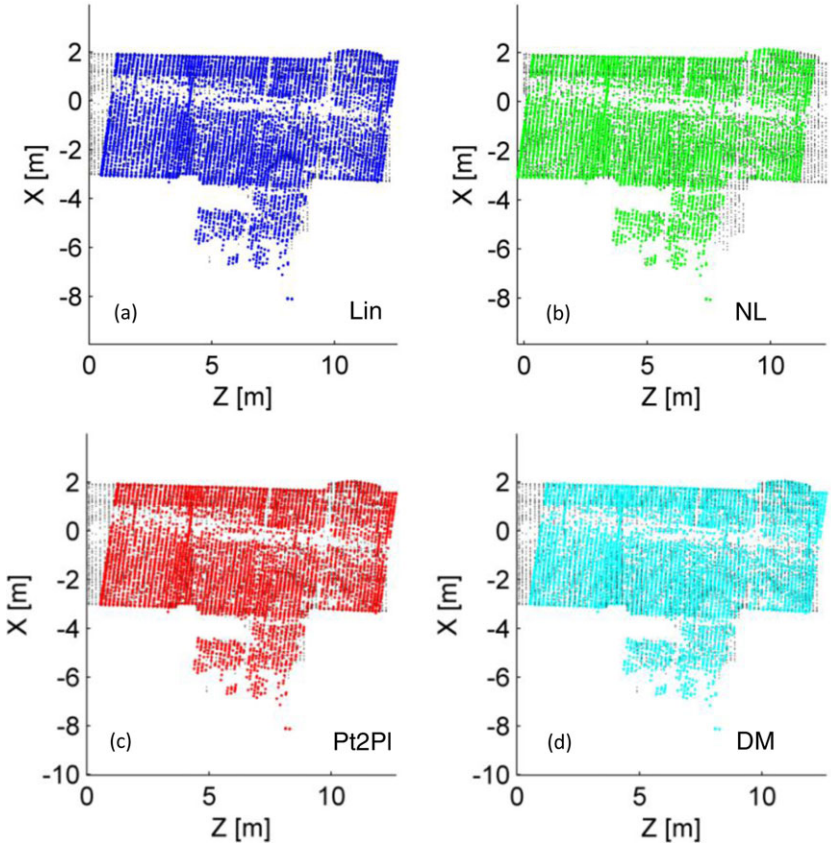

Fig. 18. Top views of the source point clouds (colored data) registered on the reference one (black data). The registration process is performed exploiting the (a) Linear ICP, (b) the Nonlinear ICP with kD-tree representation of points, (c) the standard ICP with point-to-plane metrics, and (d) the proposed ICP with deletion mask (see color figure in online version).

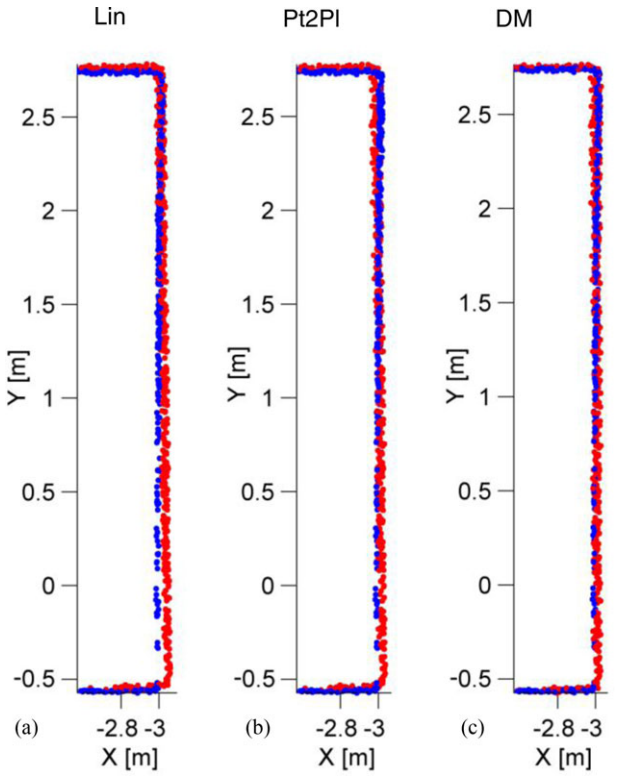

Fig. 19. Comparison of the reference point cloud (blue dots) and the registered one (red dots) extracted from the results in Figure 18. Results of (a) the Lin-ICP, (b) the Pt2Pl-ICP, and (c) DM-ICP.

registration of two point clouds obtained by the inspection of another environment, namely the entrance hall of an under-construction building, to prove the quality of the algorithm. The specific entrance hall constitutes a challenging indoor environment because of its spatial uniformity due to the lack of pillars, whose shapes and position were highly informative in the previous registrations.

As already discussed for the previous investigations, the experiment has been performed by changing the pose assumed by the vehicle before starting its movement: two point clouds model the same environment from different points of view. Figure 17 shows the two point clouds extracted from the inspection of the entrance hall and referred to the local reference system of the corresponding acquisition.

Also in this case, the proposed method for point cloud registration has been compared with the three considered ICP implementations (Lin, NL, and Pt2Pl), giving rise to the results in Figure 18, which plots separately the top views of the source point clouds, registered on the reference one.

At first glance, the qualitative inspection of outcomes prove that the NL-ICP returns the worst results among the implemented methods. On the contrary, the Lin-ICP, the Pt2Pl-ICP, and the DM-ICP perform good registrations, because the source point cloud well-matches the reference one.

With more details, Figure 19 highlights the differences between the reference data set and the source one registered by means of the Lin-ICP, the Pt2Pl-ICP, and the proposed method. The focus on Figure 19 reveals that the Lin-ICP can poorly register the input data sets. On the other hand, the Pt2Pl-ICP and the proposed DM-ICP are in good agreement with comparable results, although the DM-ICP makes use of a simpler distance metrics and a registration scheme dealing with three parameters. Quantitatively, the three correction parameters found by the Pt2Pl-ICP are $X_0 =$ 810.92 mm, $Z_0 =$ 1089.96 mm, and $H_0 =$ –8.12°, whereas the DM-ICP returns $X_0 =$ 813.48 mm, $Z_0 =$ 1071.09 mm, and $H_0 =$ −8.18°. Here, differences between corresponding parameters are negligible, because these terms are slightly higher than the measurement uncertainty of the sensor.

In summary, as stated by the inspection of the previous experiments, it is possible to envisage even better results by implementing in the proposed algorithm the point-to-plane distance metrics, which weights correspondences between points on the similarities between planes.

4 CONCLUSIONS

In this article, a numerical approach for point cloud registration returned by a laser rangefinder has been presented. The analysis has been focused on the topic of remote sensing of indoor civil infrastructures, where standard approaches based on GPS are no longer available. Acquisitions are thus referred to a local reference system having origin in the starting position of the vehicle that carries the sensor. In this case, occlusions can emerge when the point of view of the sensor changes, and thus consecutive reconstructions of the same environment can suffer from implicit differences. For this reason deletion masks have been introduced iteratively within the standard ICP technique to delete those points that can induce erroneous registrations. The method has been applied for the registration of data sets extracted from actual environments, namely a covered parking area and an entrance hall, where scenes are equal or slightly altered. Several comparisons with three well-known ICP variants have been performed by computing the distances between distinguishable markers extracted from the reference data set and the registered ones. Outcomes have proved a reduction of

the registration errors, with respect to the other implemented ICP variants. Only the use of the point-to-plane distance metrics between the data sets has lowered the negative effects of erroneous correspondences, with results often similar to those of the presented method, which implements the simpler point-to-point metrics. This behavior suggests that future developments of the method will use a more effective error metrics to further minimize the negative effects of wrong point correspondences. Finally, additional contributions will be dedicated to the reduction of the computational time required by the creation of the deletion masks. As an example, pre-computed look-up tables can be loaded at each iteration to speed up the algorithm.

ACKNOWLEDGMENTS

This work is within the CNR-ISSIA Project "MASSIME: Innovative mechatronic security systems (wired and wireless) for railway, aerospace and robotic applications" (Ref. Miur PON 02_00675). The authors would like to thank Mr. Michele Attolico for his technical support.

REFERENCES

Amenta, N, Choi, S. & Kolluri, R. K. (2001), The power crust, unions of balls, and the medial axis transform, *Computational Geometry*, **19**(2-3), 127–53.

Arka, D. (2005), Registration of point clouds using range and intensity information, in *Proceedings of the International Workshop on Recording, Modeling and Visualization of Cultural Heritage*, Centro Stefano Franscini, Monte Verita, Ascona, Switzerland, May 22-27, 2005, 141–56.

AR4000 Laser Rangefinder (2014), Available at: http://www.acuitylaser.com/laser˙rangefinders.html, accessed February 2014.

Bernardini, F., Mittleman, J., Rushmeier, H., Silva, C. & Taubin, G. (1999), The ball-pivoting algorithm for surface reconstruction, *IEEE Transactions on Visualization and Computer Graphics*, **5**(4), 349–59.

Besl, P. J. & McKay, N. D. (1992), A method for registration of 3-D shapes, *IEEE Transactions on Pattern Analysis and Machine Intelligence*, **14**(2), 239–56.

Blais, G. & Levine, M. D. (1995), Registering multiview range data to create 3D computer objects, *IEEE Transactions on Pattern Analysis and Machine Intelligence*, **17**(8), 820–24.

Cai, H. & Rasdorf, W. (2007) Modeling road centerlines and predicting lengths in 3-D using LIDAR point cloud and planimetric road centerline data, *Computer-Aided Civil and Infrastructure Engineering*, **23**(3), 157–73.

Cazzaniga, N. E., Forlani, G. & Roncella, R. (2007), Improving the reliability of a GPS/INS navigation solution for MM vehicles by photogrammetry, in *Proceedings of the 5th International Symposium on Mobile Mapping Technology*, Padua, Italy.

Chen, Y. & Medioni, G. (1991), Object modeling by registration of multiple range images, in *IEEE International Conference on Robotics and Automation*, **3**, 2724–9.

Cord, A. & Chambon, S. (2012), Automatic road defect detection by textural pattern recognition based on AdaBoost, *Computer-Aided Civil and Infrastructure Engineering*, **27**, 244–59.

Deshpande, S. S. (2013), Improved floodplain delineation method using high-density LiDAR data, *Computer-Aided Civil and Infrastructure Engineering*, **28**(1), 68–79.

Diosi, A. & Kleeman, L. (2005), Laser scan matching in polar coordinates with application to SLAM, in *Proceedings of the IEEE/RSJ International Conference on Intelligent Robots and Systems*, Shaw Convention Center-Edmonton, AB, Canada, August 2–6, 2005, 3317–22.

Dorai, C., Wang, G., Jain, A. K. & Mercer, C. (1996), From images to models: automatic 3D object model construction from multiple views, in *Proceedings of the 13th International Conference on Pattern Recognition*, **1**, 770–74.

Fitzgibbon, A. W. (2003), Robust registration of 2D and 3D point sets, *Image and Vision Computing*, **21**(13), 1145–53.

Gelfand, N., Ikemoto, L., Rusinkiewicz, S. & Levoy, M. (2003), Geometrically stable sampling for the ICP algorithm, in *Proceedings of the 4th International Conference on 3-D Digital Imaging and Modeling*, Banff, Canada, 260–67.

Gomez-García-Bermejo, J. & Zalama, E. (2013), Automated registration of 3D scans using geometric features and normalized color data, *Computer-Aided Civil and Infrastructure Engineering*, **28**, 98–111.

Grinstead, B., Sukumar, S., Page, D., Koschan, A., Gorsich, D. & Abidi, M. A. (2006), Mobile scanning system for the fast digitization of existing roadways and structures. *Sensor Review*, **26**(4), 283–9.

Han, J. Y., Guo, J. & Jiang, Y. S. (2013), Monitoring tunnel deformations by means of multi-epoch dispersed 3D LiDAR point clouds: an improved approach, *Tunnelling and Underground Space Technology*, **38**, 385–9.

Hähnel, D., Thrun, S. & Burgard, W. (2003), An extension of the ICP algorithm for modeling nonrigid objects with mobile robots, in *International Joint Conference on Artificial Intelligence*, Acapulco, Mexico, 915–20.

Holz, D. & Behnke, S. (2010), Sancta simplicitas - on the efficiency and achievable results of SLAM using ICP-based incremental registration, in *Proceedings of the IEEE International Conference on Robotics and Automation*, Anchorage, AK, May 3-8, 2010, 1380–87.

Holz, D. & Behnke, S. (2014), Registration of non-uniform density 3D point clouds using approximate surface reconstruction, in *Proceedings of the International Symposium on Robotics*, Messe München, Munich, Germany, June 2-3, 2014 .

Horn, B. K. P. (1979), SEQUINS and QUILLS representation for surface topography, in *Artificial Intelligence Memo*, Artificial Intelligence Laboratory, MIT, Cambridge, MA, no. 536.

Huber, D. F. & Hebert, M. (2003), Fully automatic registration of multiple 3D data sets, *Image and Vision Computing*, **21**(7), 637–50.

Jaboyedoff, M., Oppikofer, T., Abellán, A., Derron, M. H., Loye, A., Metzger, R. & Pedrazzini, A. (2007), Use of LIDAR in landslide investigations: a review, *Natural Hazards*, **6**(1), 5–28.

Johnson, A. E. & Sing Bing Kang (1997), Registration and integration of textured 3-D data, in *Proceedings of the International Conference on Recent Advances in 3-D Digital Imaging and Modeling*, Ottawa, Ontario, Canada, 234–41.

Kang, Z., Tuo, L. & Zlatanova, S. (2012), Continuously deformation monitoring of subway tunnel based on terrestrial point clouds, in *Proceedings of the XXII Congress of the International Society for Photogrammetry and Remote Sensing (ISPRS)*, IAPRS XXXIX-B5, Melbourne, Australia, August 25– September 1, 2012 .

Kazhdan, M., Bolitho, M. & Hoppe, H. (2006), Poisson surface reconstruction, in *Proceedings of the 4th Eurographics Symposium on Geometry Processing*, Cagliari, Italy, **7**.

Kazhdan, M. & Hoppe, H. (2013), Screened Poisson surface reconstruction, *ACM Transactions on Graphics*, **32**(3), 29.

Liu, Y. (2004), Improving ICP with easy implementation for free-form surface matching, *Pattern Recognition*, **37**(2), 211–26.

Low, K. (2004), *Linear Least-Squares Optimization for Point-to-Plane ICP Surface Registration*, Technical Report, Department of Computer Science, University of North Carolina, Chapel Hill, NC, TR04–004.

Marani, R., Roselli, G., Nitti, M., Cicirelli, G., D'Orazio, T. & Stella, E. (2013), Analysis of indoor environments by range images, in *Proceedings of the 7th International Conference on Sensing Technology*, Massey University, Wellington, New Zealand, December 3–5, 2013, 163–8.

Mitra, N. J., Nguyen, A. & Guibas, L. (2004), Estimating surface normals in noisy point cloud data, *International Journal of Computational Geometry & Applications*, **14**(04n05), 261–76.

Moenning, C. & Dodgson, N. A. (2004), Intrinsic point cloud simplification, in *GraphiCon*, Moscow, Russia.

Moreno, F.-A., Gonzalez-Jimenez, J. & Blanco, J.-L. (2013), An instrumented vehicle for efficient and accurate 3D mapping of roads, *Computer-Aided Civil and Infrastructure Engineering*, **28**, 403–19.

Murray, R. M., Li, Z. & Sastry, S. S. (1994), *A Mathematical Introduction to Robotic Manipulation*, CRC Press, Taylor and Francis Group, Boca Raton, FL.

Nishikawa, T., Yoshida, J., Sugiyama, T. & Fujino, Y. (2012), Concrete crack detection by multiple sequential image filtering, *Computer-Aided Civil and Infrastructure Engineering*, **27**, 29–47.

Ohtake, Y., Belyaev, A., Alexa, M., Turk, G. & Seidel, H. P. (2003), Multi-level partition of unity implicits, in *Proceedings of the 30th International Conference on Computer Graphics and Interactive Techniques*, San Diego, California, 173–80.

Park, H. S., Lee, H. M., Adeli, H. & Lee, I. (2007), A new approach for health monitoring of structures: terrestrial laser scanning, *Computer-Aided Civil and Infrastructure Engineering*, **22**, 19–30.

Park, S. W., Park, H. S., Kim, J. H. & Adeli, H. (2015), 3D displacement measurement model for health monitoring of structures using a motion capture system, *Measurement*, **59**, 352–62.

Pfeifer, N. & Böhm, J. (2008), Early stages of LiDAR data processing, in Li, Z., Chen, J. & Baltsavias, E. (eds.), *Advances in Photogrammetry, Remote Sensing and Spatial Information Sciences*, 2008 ISPRS Congress Book, pp. 169–84.

Pomerleau, F., Colas, F., Siegwart, R. & Magnenat, S. (2013), Comparing ICP variants on real-world data sets, *Autonomous Robots*, **34**(3), 133–48.

Ramer, U. (1972), An iterative procedure for the polygonal approximation of plane curves, *Computer Graphics and Image Processing*, **1**(3), 244–56.

Rowekamper, J., Sprunk, C., Tipaldi, G. D., Stachniss, C., Pfaff, P., Burgard, W. (2012), On the position accuracy of mobile robot localization based on particle filters combined with scan matching, in *Proceedings of the IEEE/RSJ International Conference on Intelligent Robots and Systems*, Vilamoura, Algarve, Portugal, October 7–12, 2012, 3158–64.

Rusinkiewicz, S. & Levoy, M. (2001), Efficient variants of the ICP algorithm, in *Proceedings of the 3rd International Conference on 3-D Digital Imaging and Modeling*, Quebec City, Quebec, Canada, 145–52.

Rusu, R. B. & Cousins, S. (2011), 3d is here: point cloud library (pcl), in *Proceedings of the IEEE International Conference on Robotics and Automation*, International Conference Center, Shanghai, China, 1–4.

Rusu, R. B., Marton, Z. C., Blodow, N., Dolha, M. & Beetz, M. (2008), Towards 3D point cloud based object maps for household environments, *Robotics and Autonomous Systems*, **56**(11), 927–41.

Scaioni, M., Barazzetti, L., Giussani, A., Previtali, M., Roncoroni, F. & Alba, M. I. (2014), Photogrammetric techniques for monitoring tunnel deformation, *Earth Science Informatics*, **7**(2), 83–95.

Sharp, G. C., Lee, S. W. & Wehe, D. K. (2002), ICP registration using invariant features, *IEEE Transactions on Pattern Analysis and Machine Intelligence*, **24**(1), 90–102.

Song, H. & Feng, H.-Y. (2009), A progressive point cloud simplification algorithm with preserved sharp edge data, *The International Journal of Advanced Manufacturing Technology*, **45**, 583–92.

Truong-Hong, L., Laefer, D. F., Hinks, T. & Carr, H. (2013), Combining an angle criterion with voxelization and the flying voxel method in reconstructing building models from LiDAR data, *Computer-Aided Civil and Infrastructure Engineering*, **28**(2), 112–29.

Walsh, S. B., Borello, D. J., Guldur, B. & Hajjar, J. F. (2013), Data processing of point clouds for object detection for structural engineering applications, *Computer-Aided Civil and Infrastructure Engineering*, **28**, 495–508.

Whelan, T., Ma, L., Bondarev, E., de With, P. H. N. & McDonald, J. (2015), Incremental and batch planar simplification of dense point cloud maps, *Robotics and Autonomous Systems*, **69**, 3–14.

Xin, W. & Pu, J. (2010), An Improved ICP Algorithm for Point Cloud Registration, in *Proceedings of the International Conference on Computational and Information Sciences*, Chengdu, Sichuan, China, December 17–19, 2010, 565–68.

Zhang, C. & Elaksher, A. (2012), An unmanned aerial vehicle-based imaging system for 3D measurement of unpaved road surface distresses, *Computer-Aided Civil and Infrastructure Engineering*, **27**, 118–29.

APPENDIX

ANALYTICAL FORMULATION FOR VIRTUAL MEASUREMENTS

Referring to the sketch in Figure A1, the positions where the environment is virtually sensed are described by the generic direction of the unit vector $\mathbf{u} = [u_x, u_y, u_z]^T$, having $u_x^2 + u_y^2 + u_z^2 = 1$. Specifically, these

positions are obtained by dividing the corresponding line τ in $(S+1)$ points p_s, with $s = 0, \ldots, S$, starting from $p_0 = [x_0, y_0, z_0]^T$, origin of $\mathbf{u}$, till p_S (end of the domain). It is easy to demonstrate that the formulation of the line τ can be written as:

$$\tau : \begin{cases} u_z (x - x_0) = u_x (z - z_0) \\ u_z (y - y_0) = u_y (z - z_0) \end{cases} \quad \text{(A.1)}$$

It follows that the generic point of view p_s, origin of the numerical resampling of the surfaces, is placed at coordinates:

$$p_s = [x_0 + s\,\Delta p\,u_x,\ y_0 + s\,\Delta p\,u_y,\ z_0 + s\,\Delta p\,u_z]^T \quad \text{(A.2)}$$

being Δp the sampling interval of the line τ.

Once these positions are determined, the surroundings can be resampled by considering the intersection between a line, orthogonal to τ and swept through 360 degrees around τ by steps of Δt, and the corresponding triangular patch of the surface set $\mathbf{S}_i$.

Analytically, the problem of virtual resampling consists in finding the point $\overline{p^f_{s,t}}$ where the line $\upsilon^{\mathbf{u}}_{s,t}$ on the plane π_s intercepts the triangle π^f (pink patch in Figure A1). Hereafter, $t = 0, \ldots, T$ is related to the specific discrete angle θ_t, which describes the slope of the line $\upsilon^{\mathbf{u}}_{s,t}$ on π_s. Notice that $Q = (S+1)\cdot T$.

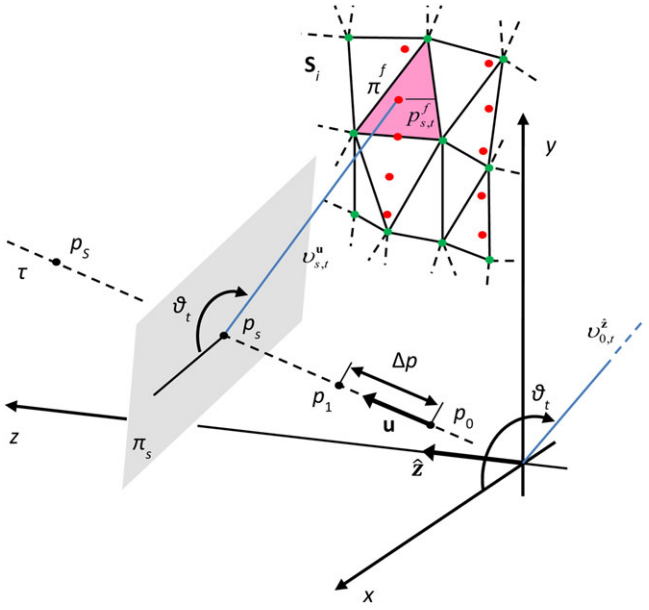

Fig. A1. Scheme of principle for the virtual measurement. Red dots on the surface set $\mathbf{S}_i$ are the results of the discrete resampling along the direction of the vector $\mathbf{u}$, whereas the green dots are the points of the initial data set (see color figure in online version). The sketch also reports the main parameters and variables of the presented formulation for virtual resampling.

The main idea for determining the equation of $\upsilon^{\mathbf{u}}_{s,t}$ is to start with the formulation of the line $\upsilon^{\hat{\mathbf{z}}}_{0,t}$, which belongs to a set of lines able to divide the xy-plane in T equally spaced portions around the z-axis, and crosses the origin of the system of coordinates (x, y, z). Then applying a transformation of reference systems, $\upsilon^{\hat{\mathbf{z}}}_{0,t}$ can be moved onto π_s, obtaining the equation of $\upsilon^{\mathbf{u}}_{s,t}$. It is straightforward to verify that $\upsilon^{\hat{\mathbf{z}}}_{0,t}$ has formulation:

$$\upsilon^{\hat{\mathbf{z}}}_{o,t} : \begin{cases} \sin\theta_t x - \cos\theta_t y = 0 \\ z = 0 \end{cases} \quad \text{(A.3)}$$

Knowing the components of the unit vector $\mathbf{u}$, it is possible to couple a rotation matrix $\mathbf{R}$ able to transform the versor $\hat{\mathbf{z}}$, element of the basis of the coordinate system (x, y, z), into a new vector having the same origin, but parallel to τ. Taking advantage of the well-known Rodrigues' formula (Murray et al., 1994), the term responsible for the rotation of $\hat{\mathbf{z}}$ onto the direction of $\mathbf{u}$ is:

$$\mathbf{R}^{\mathbf{u}}_{\hat{\mathbf{z}}} = \begin{bmatrix} 1 - \dfrac{1-u_z}{u_x^2+u_y^2}u_x^2 & -\dfrac{1-u_z}{u_x^2+u_y^2}u_x u_y & u_x \\ -\dfrac{1-u_z}{u_x^2+u_y^2}u_x u_y & 1 - \dfrac{1-u_z}{u_x^2+u_y^2}u_y^2 & u_y \\ -u_x & -u_y & u_z \end{bmatrix} \quad \text{(A.4)}$$

The analytical formulation of the sampling line $\upsilon^{\mathbf{u}}_{s,t}$ can be thus obtained by applying a $\mathbf{R}^{\mathbf{u}}_{\hat{\mathbf{z}}}$-rotation of the fundamental line $\upsilon^{\hat{\mathbf{z}}}_{0,t}$ and a rigid translation on the specific point of view p_s.

Applying the presented transformation, $\upsilon^{\mathbf{u}}_{s,t}$ can be written as:

$$\upsilon^{\mathbf{u}}_{s,t} : \begin{cases} \dfrac{(u_x + u_y\tan\theta_t)(x - x_0 - s\Delta p u_x)}{z - z_0 - s\Delta p u_z} \\ \quad = \dfrac{1-u_z}{u_x^2+u_y^2}u_x^2 + \dfrac{1-u_z}{u_x^2+u_y^2}u_x u_y \tan\theta_t - 1 \\ \dfrac{(u_x + u_y\tan\theta_t)(y - y_0 - s\Delta p u_y)}{z - z_0 - s\Delta p u_z} \\ \quad = \dfrac{1-u_z}{u_x^2+u_y^2}u_y^2 \tan\theta_t + \dfrac{1-u_z}{u_x^2+u_y^2}u_x u_y - \tan\theta_t \end{cases} \quad \text{(A.5)}$$

Then, the generic sampling line can be tested to find the target point $\overline{p^f_{s,t}}$ among all the possible intersections of $\upsilon^{\mathbf{u}}_{s,t}$ with the planes of the triangles which form the set of surfaces $\mathbf{S}_i$. The fth triangle belonging to $\mathbf{S}_i$, $f = 1, \ldots, F$, being F the number of triangles, is defined by an ordered set of three vertices (v^f_1, v^f_2, v^f_3), each one having coordinates (x^f_a, y^f_a, z^f_a), with $a = 1, 2, 3$. When the vertices are known, the equation of the plane π^f can be derived as well as the coordinates of the points $p^f_{s,t}$, which are the intersections between $\upsilon^{\mathbf{u}}_{s,t}$ and any plane π^f. As stated previously, there is only one point $\overline{p^f_{s,t}}$, among the

set of F possible points $p^f_{s,t}$, which is a valid solution for the resampling problem: if the intersection returns a point falling within the triangle sides, $\overline{p^f_{s,t}}$ is a sample of the data set.

This condition can be verified by testing whether $p^f_{s,t}$ is inside the spatial region bounded by the three planes $\pi^{f,\perp}_{12}$, $\pi^{f,\perp}_{23}$ and $\pi^{f,\perp}_{13}$, orthogonal to the plane π^f and including the couples of points (v^f_1, v^f_2), (v^f_2, v^f_3), and (v^f_1, v^f_3), respectively. Equivalently, given three numbers $\alpha \neq \beta \neq \gamma$, with $\alpha = 1, 2$ and $\beta = 2, 3$, this condition requires that the possible point $p^f_{s,t}$ and the vertex v^f_γ are both placed in the same hemispace generated by the plane $\pi^{f,\perp}_{\alpha\beta}$. Analytically, the point $\overline{p^f_{s,t}}$ satisfies the following:

$$\begin{cases} \operatorname{sgn}\left(\pi^{f,\perp}_{12}\left(v^f_3\right)\right) \cdot \pi^{f,\perp}_{12}\left(\overline{p^f_{s,t}}\right) > 0 \\ \operatorname{sgn}\left(\pi^{f,\perp}_{23}\left(v^f_1\right)\right) \cdot \pi^{f,\perp}_{23}\left(\overline{p^f_{s,t}}\right) > 0 \\ \operatorname{sgn}\left(\pi^{f,\perp}_{13}\left(v^f_2\right)\right) \cdot \pi^{f,\perp}_{13}\left(\overline{p^f_{s,t}}\right) > 0 \end{cases} \tag{A.6}$$

where $\operatorname{sgn}(\cdot)$ is the sign function and $\pi(p)$ is the result of the application of the point p to the equation of the plane π.

Finally, given the coordinates of $\overline{p^f_{s,t}}$, the radial component can be easily determined, thus obtaining the effective virtual range measurement $\rho^v_{i,j}(\mathbf{u})$ in the reference system described by $\mathbf{u}$ and centered on p_s.